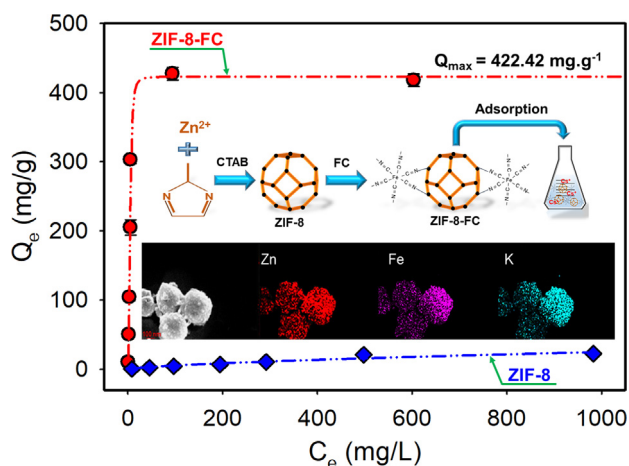# Caesium adsorption on a zeolitic imidazolate framework (ZIF-8) functionalized by ferrocyanide

Quynh Thi Ngoc Le [a], Kuk Cho [a,*]

[a] Department of Environmental Engineering, Pusan National University, 2, Busandaehak-ro 63beon-gil, Geumjeong-gu, Busan 46241, Republic of Korea

GRAPHICAL ABSTRACT

ARTICLE INFO

ABSTRACT

^{137}Cs is one of the most hazardous radionuclides in nuclear waste owing to its toxicity. Developing an adsorbent for Cs^+ with a high capacity and selectivity is a challenging task. A metal–organic framework (MOF) is a material with a high surface area that has been widely applied in wastewater treatment. Exploiting the affinity between ferrocyanide (FC) and Cs^+, zeolitic imidazolate framework-8 (ZIF-8) was chemically functionalized with FC, ZIF-8-FC to selectively capture Cs^+. After functionalization, ZIF-8-FC has a hollow morphology and small FC related crystals, which might result in better migration of Cs^+ inside ZIF-8-FC. This synergistic effect was proven by the Q_{max} of ZIF-8-FC, 422.42 mg g^{-1}, which is 15.9 times higher than that of ZIF-8. Additionally, ZIF-8-FC retained its good adsorption performance within a pH range of 3–11 and an excellent Cs^+ selectivity even in artificial seawater conditions. The structure of ZIF-8-FC after adsorption proves its stability. Furthermore, the thermodynamic adsorption implied that higher temperatures are more favorable for Cs^+ uptake. This work demonstrates the remarkable adsorption and selectivity of ZIF-8-FC, which make it a promising candidate for remediation of radioactive Cs^+.

* Corresponding author.
  E-mail address: kukcho@pusan.ac.kr (K. Cho).

1. Introduction

The use of nuclear energy is globally increasing; consequently, fission products in nuclear wastewater have attracted significant concern due to their detrimental environmental effects. In addition, following the nuclear accidents at Three Mile Island in the USA (1979), Chernobyl in Ukraine (1986), and Fukushima Daiichi in Japan (2011), fission products released into the environment have severely contaminated rivers, groundwater, and seawater [1–3]. Among the common fission products, ^{137}Cs is one of the most hazardous, and it has attracted significant concern owing to its half-life of approximately 30 years and its strong β–γ emissions [4]. Because Cs has metabolic and chemical properties similar to those of K and Na, it can be easily deposited in tissues once introduced to the human body, causing a long-term radiation exposure, which could eventually lead to cancer, genic mutations, leukemia, and other diseases [5,6]. Therefore, using efficient technology to remove Cs from water is of paramount importance.

Researchers have employed various techniques to separate Cs from aqueous solutions, including precipitation [7], ultrafiltration [8] solvent extraction [9], and adsorption [10]. Among them, adsorption is a feasible method owing to its high efficiency, simplicity, and ecofriendliness [3,11,12]. Over the past few decades, a broad range of ion-exchange adsorbents, such as zeolite [13], metal sulfides [14–16], clay [10], transition metal ferrocyanides (MFCs) [2], and titanium silicate [17] have been explored to remove Cs^+. The general formula of MFC is $A_xM_y[Fe(CN)_6]_z \cdot nH_2O$, where A is the alkali cation (A = K^+, Na^+) and M is the transition metal cation (M = Ni^{2+}, Co^{2+}, Cu^{2+}, Zn^{2+}, etc.). Cs^+ can replace these alkali metal cations owing to the high affinity between Cs^+ and ferrocyanide (FC). Furthermore, the MFC channel size, which is 3.2 Å, is suitable for hydrated Cs^+ [10]. Therefore, MFCs have a high selectivity for Cs^+ compared to those of competing ions, such as Na^+ and K^+ [18].

Recently, metal–organic frameworks (MOFs) have attracted attention as promising adsorbents owing to their highly porous structures and tunable sizes [19,20]. Several publications have described the use of MOFs as adsorbents for Cs^+ ions, including MIL-101-SO_3H [21], HKUST-1/KNiFC [22], InMOF [23] and Uranyl MOFs [3,24]. However, these MOFs have the disadvantages of low selectivity for Cs^+, low maximum adsorption capacities, and/or cumbersome processes involving high temperatures and a synthesis that requires long time periods, sometimes spanning one week. These shortcomings limit their potential large-scale application as highly efficient adsorbents. Thus, we studied the synthesis of a new MOF with a high maximum adsorption capacity and selectivity at room temperature.

The zeolitic imidazolate framework-8 (ZIF-8) is a strong candidate for achieving these objectives owing to its simple synthesis conditions, excellent chemical stability, and high mechanical strength [25–27]. ZIF-8 has been used to remove UO^{2+} [27], Cr (VI) [28], and Pb^{2+} [29]; however, to the best of our knowledge, it has not been used to remove Cs^+. In addition, we are the first to synthesize a MOF material chemically functionalized with FC, which offers a high adsorption capacity, selectivity, and easy synthesis. A simple mixture of MOF/MFC has been reported as HKUST-1/KNiFC [22]. However, in this case, HKUST-1 and KNiFC were synthesized separately and were mixed afterward. This simple mixture explains its lower maximum adsorption capacity of 153 mg g^{-1} and lower selectivity, compared to those of pure KNiFC.

In this study, ZIF-8 functionalized with FC (ZIF-8-FC) was successfully synthesized at room temperature following simple steps and was used to adsorb Cs^+ from an aqueous solution. The factors that influenced the removal properties, including the pH, adsorption time, temperature, and competing ions were investigated.

ZIF-8-FC exhibited a remarkable adsorption performance and high selectivity for Cs^+; therefore, it is a promising candidate for the remediation of radioactive Cs^+.

2. Material and methods

2.1. Chemicals and materials

The compound, 2-methylimidazole (2-MeIm), was purchased from FUJIFILM Wako Pure Chemical Co. (Japan). Caesium nitrate ($CsNO_3$, 99.8% metal basis) was purchased from Alfa Aesar (USA). Zinc nitrate hexahydrate ($Zn(NO_3)_2 \cdot 6H_2O$, 98%), potassium ferrocyanide trihydrate (($K_4Fe(CN)_6) \cdot 6H_2O$, 99%), cetyltrimethylammonium bromide (CTAB, 99%), methyl alcohol (CH_3OH, 99.8%), sodium chloride (NaCl, 99.5%), potassium chloride (KCl, 99%), magnesium chloride hexahydrate ($MgCl_2 \cdot 6H_2O$, 98%), calcium chloride ($CaCl_2$, 99%) and hydrochloric acid (HCl, 37%) were purchased from Daejung Chemicals and Metals Co. Ltd. (South Korea). Sodium hydroxide (NaOH, 98%) was purchased from Samchun Chemical Co. Ldt. (South Korea). ASW was purchased from Coralife (USA). All chemicals were used without further purification.

2.2. Material synthesis

2.2.1. Synthesis of ZIF-8

ZIF-8 particles were prepared by a precipitation method slightly modified from that described in a previous study [26]. First, 2.5 mmol of $Zn(NO_3)_2 \cdot 6H_2O$ was dissolved in 100 mL of water to form a clear solution (solution A). Separately, 150 mmol of 2-MeIm and 2 mL of 0.01 M CTAB were dissolved in 100 mL of water to form a clear solution (solution B). Subsequently, solution A was quickly added to solution B under vigorous magnetic stirring. Thereafter, the mixture slurry was kept at 25 °C for 24 h for ZIF-8 crystal growth. Finally, the product was separated using a centrifuge (Combi 514R, Hanil Scientific Inc., South Korea) at 8000 rpm (7024 g-force) for 10 min and washed several times with distilled water and methanol, followed by drying overnight in a vacuum oven at 80 °C.

2.2.2. Synthesis of ZIF-8 functionalized with ferrocyanide (ZIF-8-FC)

A mass of 0.23 g of ZIF-8 was dispersed in 75 mL of methanol using an ordinary ultrasonic bath. Subsequently, 0.1 M $K_4Fe(CN)_6$ aqueous solution was injected into the ZIF-8 solution with continuous stirring at 25 °C maintained for 15 h. Various ZIF-8-FC materials were prepared at FC/ZIF-8 M ratios of 0.4, 0.8, and 2, corresponding to 4, 8 and 16 mL of 0.1 M $K_4Fe(CN)_6$ solution, respectively. The resulting solid was collected, washed, and dried in a vacuum oven at 105 °C.

2.3. Characterization

The Brunauer–Emmett–Teller (BET) method was used to measure the specific surface area and pore volume of the materials using the N_2 adsorption at 77 K (ASAP 2020, Micromeritics, USA). The functional groups of the samples were analyzed by Fourier transform infrared (FTIR) spectroscopy (IRAffinity-1, Shimadzu, Japan). The spectra were obtained by accumulating scans at a resolution of cm^{-1} in the range of 4000–500 cm^{-1}. To investigate the surface morphology of the synthesized nanoparticles, field-emission scanning electron microscopy (FE-SEM) was carried out (S-2700, Hitachi, Japan), and energy-dispersive X-ray spectroscopy (EDS) was conducted using a TESCAN system (MIRA3 LMH In-Beam, Czech Republic). An X-ray diffractometer (Xpert 3 Powder, Malvern Panalytical Ltd., U.K.) was used to identify the crystal structures of the samples. Thermogravimetric analyses (TGA) were

obtained using TGA equipment (SDT Q600, TA Instruments, USA) under atmosphere between temperatures of 20 to 700 °C.

2.4. Adsorption experiments

All the adsorption experiments were carried out at 25 °C using the batch method. The typical conditions used were as follows: V/m of 1000 mL g^{-1}, solution volume of 25 mL, initial Cs$^+$ concentration of 500 mg L^{-1}, solution pH of 7, FC/ZIF-8M ratio of 0.8, and contact time of 24 h. The Cs$^+$ solution was prepared from the 1000 mg L^{-1} stock solution by dilution. The pH of the solution was adjusted using NaOH or HCl.

The kinetic adsorption was tested for up to 24 h and the results were analyzed using the pseudo-first-order and second-order models. The adsorption isotherm was obtained by varying the initial concentration of Cs$^+$ from 10 to 1000 mg L^{-1} under 298, 308, and 318 K. All experiments were conducted in triplicates. The adsorption capacity of the materials, q_e (mg g^{-1}), was calculated based on the following equation:

$$q_e = \frac{(C_o - C_e)V}{m}, \tag{1}$$

where C_o (mg L^{-1}) and C_e (mg L^{-1}) represent the initial and equilibrium concentrations of Cs$^+$; V (L) is the volume of the solution, and m (g) is the mass of the adsorbent.

To evaluate the selectivity of ZIF-8-FC, we conducted an adsorption test in ASW. The ion components of ASW are presented in Table S1. The initial concentration of Cs$^+$ was 300 mg L^{-1}. The distribution coefficient (K_d) of the Cs adsorption on ZIF-8-FC was calculated using the following equation:

$$K_d = \frac{V}{m} \frac{C_o - C_e}{C_e} \tag{2}$$

2.5. Analysis

The liquid samples were separated after adsorption using a 0.2 μm cellulose acetate syringe filter (Advantec, Toyo Roshi Kaisha Ltd., Japan). The Cs$^+$ and K$^+$ concentrations were measured using an atomic absorption spectrometer (AAS-200, PerkinElmer Inc., USA) and ICP-MS (Nexion 2000, PerkinElmer Inc., USA). The solution pH values were measured using a pH meter (Orion Star A211, ThermoFisher Scientific, Indonesia).

3. Results and discussion

3.1. Characterization

The functional groups in the synthesized samples were analyzed, as shown in Fig. S1. The ZIF-8 spectra were consistent with those reported in previous studies [25,26]. The peaks at 694 and 770 cm^{-1} correspond to the out-of-plane bending of the 2-MeIm ring. Similarly, the peaks at 999 and 1310 cm^{-1} may be the result of in-plane bending. The peak at 1585 cm^{-1} refers to the stretching C=N vibration of 2-MeIm. The spectra of ZIF-8-FCs, at various ratios of FC to ZIF-8 from 0.4 to 2.0, contained the main peaks of the ZIF-8 spectra. Additionally, ZIF-8-FC showed new peaks at 602 and 2096 cm^{-1}. Those peaks represent the Fe—C group and the C≡N group from FC, respectively, which confirms that successful bonding occurred between ZIF-8 and FC [30].

The specific surface area (SSA) and pore volume of the samples were analyzed using the N$_2$ adsorption–desorption isotherms (Fig. 1a). The SSA of ZIF-8 was 1291 m^2 g^{-1}, which is close to the reported value of 1079 m^2 g^{-1} [31]. After functionalization with FC, the BET SSA and pore volume decreased to 589 m^2 g^{-1} and 0.41 cm^3 g^{-1}, respectively, while the FC loading increased to 2.0

(Table S2). The pore size distribution of the samples showed that all samples are mesoporous (Fig. S2). FC was coordinated with the unsaturated zinc, and subsequent ligand exchange was attributed to the formation of potassium zinc ferrocyanide (KZFC). FC blocked several of the ZIF-8 pores, which caused a decrease in the SSA and pore volume. The effect of the FC loading, SSA, and pore volume on the Cs$^+$ adsorption performance is discussed in the adsorption section.

Fig. 1b shows the XRD patterns of ZIF-8 and ZIF-8-FCs. All samples showed high intensities and flat backgrounds, which indicates that the samples had high crystallinity. The XRD patterns of ZIF-8 agrees well with those reported in previous studies [25,26]. The XRD patterns of ZIF-8-FCs coincide with the peak position of ZIF-8. The main peaks of ZIF-8 occurred in all samples, which implied that the original crystal phase of ZIF-8 was retained after the FC functionalization. However, in the ZIF-8-FC(2.0) XRD pattern, several peaks of pristine ZIF-8 disappeared, which implied that the crystallinity of ZIF-8 was reduced. After ZIF-8 was functionalized with FC, the peaks corresponding to the (0 1 1) and (1 1 2) planes shifted toward lower 2θ (higher d spacing) values because the larger FC (ionic radius of 4.35 Å) replaced several of the smaller 2-methylimidazole (ionic radius of imidazole = 2.58 Å) in the ZIF-8 structure [32,33]. At higher concentrations of FC, new peaks at 24.6°, 41.0°, and 43.2° were observed and corresponded to the (0 3 0), (1 3 1 0), and (3 3 0) planes of KZFC (ICDD 98 000 8248). The crystal size of KZFC in ZIF-8-FC(2.0) calculated using Scherrer's equation was 26 nm, which is smaller than that reported for zinc ferrocyanide (~300 nm) [34]. After the Cs$^+$ adsorption, the ZIF-8-FC(0.8) retained the original peaks, which proves that the material is stable. Moreover, the new peaks at 34.7°, 42.8°, 44.6° and 49.7° were identified as caesium zinc ferrocyanide [35] and elemental mapping is shown in Fig. S9.

A thermogravimetric analysis of ZIF-8-FC before and after adsorption (Fig. S3) shows that the samples were stable up to approximately 400 °C after which point they started to drastically decompose. Fig. 2(a–d) shows the morphologies of the samples that were investigated by FE-SEM. As shown in Fig. 2a, the ZIF-8 particles were cubic and had smooth surfaces with an average size of 400 nm. In Fig. 2b, the ZIF-8-FC(0.4) particles had a similar shape as those of ZIF-8, except for the tiny and spherical particles on the surface. The ZIF-8-FC(0.8) particles shown in Fig. 2c had more rounded shapes compared to the ZIF-8 particles, although the particle size of the former was similar to that of ZIF-8. When the FC ratio increased to 2.0, agglomerates composed of primary particles were present (Fig. 2d). Additionally, several particles had a partial defect on one side that made them hollow. FC was coordinated to unsaturated zinc in ZIF-8 and formed KZFC without disturbing the underlying coordination framework of ZIF-8 [36,37]. Then, parts of ZIF-8 were slowly decomposed, and 2-MeIm was replaced by FC through ligand exchange. This process can explain the broken or hollow morphology of ZIF-8-FC. The formed KZFC was enlarged by growth and resulted in the spherical particles on the surface of ZIF-8-FC.

SEM elemental mapping images (Fig. 2e) show that Zn, Fe and K are distributed homogeneously throughout the whole particles. The amounts of Zn, Fe, and K in ZIF-8 and ZIF-8-FCs were determined by EDS (Fig. S4). ZIF-8 showed no K and Fe content. As the FC loading increased from 0.4 to 0.8, the molar ratios of Fe/Zn increased from 0.24 to 0.56, even though the values were less than the theoretical ones. When the FC loading increased to 2.0, the ratio was 0.60, which slightly increased, implying saturation.

3.2. Adsorption

3.2.1. Optimum ratio of FC to ZIF-8

As the ratio of FC to ZIF-8 increased from 0.4 to 0.8, the adsorption capacity increased from 257.41 ± 1.61 mg g^{-1} to 427.38 ± 9.
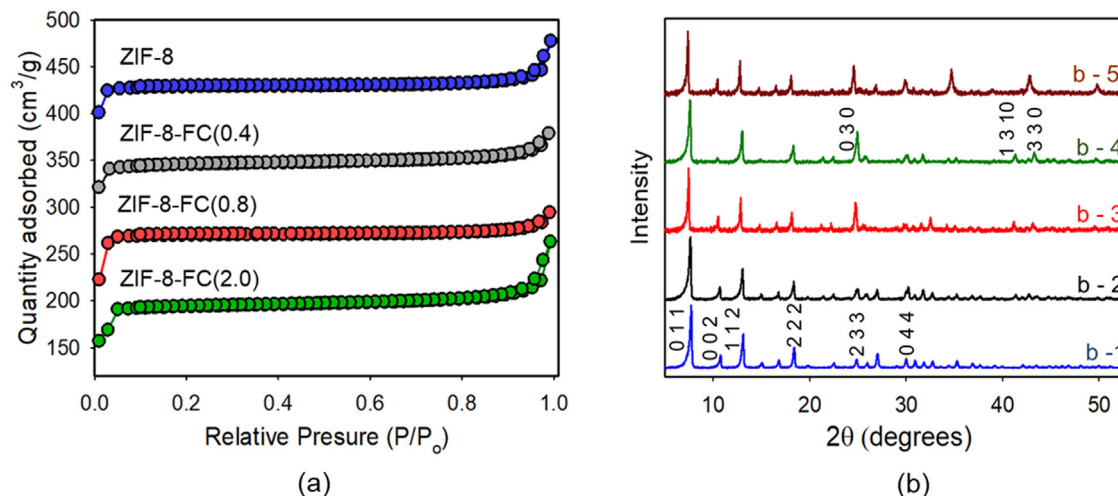
Fig. 1. (a) Nitrogen adsorption–desorption isotherms, and (b) XRD spectra of (b-1) ZIF-8, (b-2) ZIF-8-FC(0.4), (b-3) ZIF-8-FC(0.8), (b-4) ZIF-8-FC(2.0), and (b-5) ZIF-8-FC(0.8) after Cs^+ adsorption.
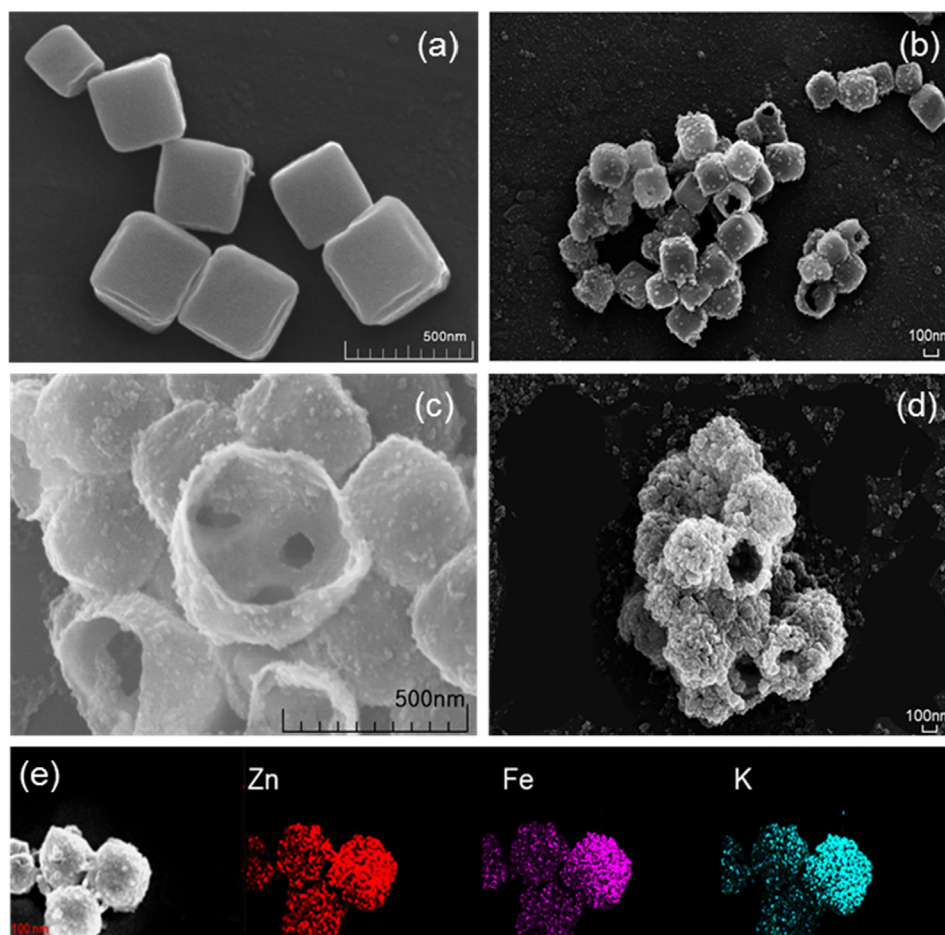

Fig. 2. FE-SEM images of (a) ZIF-8; (b) ZIF-8-FC(0.4); (c) ZIF-8-FC(0.8); (d) ZIF-8-FC(2.0), respectively, and (e) elemental mapping of ZIF-8-FC(0.8).

34 mg g^{-1} (Fig. 3a). This proved that the ZIF-8-FC(0.8) composite had a higher Cs^+ uptake relative to that of ZIF-8-FC(0.4), which was attributed to the higher availability of FC in ZIF-8-FC(0.8). However, with a further increase in the FC ratio to 2.0, the adsorption capacity decreased to 368.71 ± 11.9 mg g^{-1}. This may be attributed to the smaller SSA and pore volume values that originated from the blockage of the porous structure of ZIF-8-FC by

excess FC compounds. Therefore, the ZIF-8-FC(0.8) composite was used in further experiments.

3.2.2. Effect of pH

The pH values of radioactive wastewater are variable. We tested the adsorption capacity of ZIF-8 and ZIF-8-FC at various pH values, ranging from 3 to 11, as shown in Fig. 3b. The adsorption capacity
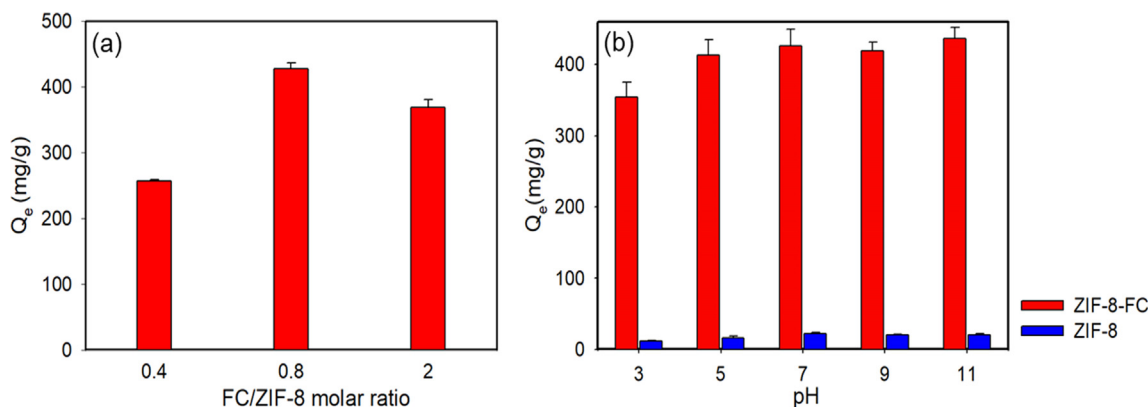
Fig. 3. The adsorption capacity of Cs⁺: (a) at various molar ratios of FC, and (b) at various pH values (C_o = 500 mg L^{-1}, V/m = 1000 mL g^{-1}, contact time = 24 h, T = 298 K).

of ZIF-8-FC was over 400 mg g^{-1} at a pH range of 5–11. Although the adsorption capacity was relatively low at pH 3, it was still above 350 mg g^{-1}. This is an advantage of ZIF-8-FC, as, generally, nuclear wastewater is alkaline [21]. The relatively low uptake capacity at pH 3 can be attributed to the inhibition of Cs⁺ adsorption by the large quantity of H⁺ present in the solution. Furthermore, the protonated surface caused an electrostatic repulsion of Cs⁺[22]. However, ZIF-8-FC still exhibited a remarkable Cs⁺ capture capacity of 354 ± 20.82 mg g^{-1} at pH 3. This implies that the ZIF-8-FC material can adsorb Cs⁺ from solutions over a relatively wide pH range of 3–11. A pH of 7 was chosen for further experiments.

3.2.3. Kinetic adsorption

Kinetic adsorptions were performed to investigate the adsorption rate of Cs⁺. The concentration of Cs⁺ removed by ZIF-8-FC rapidly decreased, and the removal efficiency reached 60% and 85% at 3 h and 24 h, respectively (Fig. S5a). As shown in Fig. 4a, the Cs⁺ uptake on ZIF-8 and ZIF-8-FC rapidly increased during the first 3 h and slowly increased afterward. After 24 h, the adsorption capacity of ZIF-8-FC was greater than 400 mg g^{-1}. Conversely, the adsorption capacity of ZIF-8 was very low.

The data were analyzed based on the pseudo-first-order and pseudo-second-order models [38]. The linear equations are as follows.

Pseudo-first-order:

$$\ln(q_e - q_t) = \ln q_e - K_1 t. \tag{3}$$

Pseudo-second-order:

$$\frac{t}{q_t} = \frac{1}{K_2 q_e^2} + \frac{t}{q_e}, \tag{4}$$

where q_t (mg g^{-1}) and q_e (mg g^{-1}) are the amounts of Cs⁺ adsorbed at time t (min) and at equilibrium, respectively. K_1 is the pseudo-first-order rate constant (min^{-1}) and K_2 is the pseudo-second-order rate constant (g mg^{-1} min^{-1}).

The calculated parameters of both kinetic models are listed in Table 1, Fig. 4b and Fig. S5b. Both ZIF-8-FC and ZIF-8 showed a better correlation with the pseudo-second-order model. This implies that the adsorption procedure depended on the number of active sites on the adsorbent. The rate-limiting step may involve chemical adsorption by sharing or exchange of electrons or ions between the adsorbent and adsorbate [1,23,38,39]. Moreover, Table 1 shows that a significant improvement occurred in the adsorption of Cs⁺ on the framework of ZIF-8 functionalized with FC.

3.2.4. Adsorption isotherm

To evaluate the maximum Cs⁺ adsorption capacity of ZIF-8-FC, detailed isotherm experiments were carried out at room temperature. In addition, the maximum adsorption capacity (q_m) of this material was compared with those of ZIF-8 and other adsorbents. The Cs⁺ adsorption isotherm data were fitted with the nonlinear forms of Langmuir, Freundlich and Sips adsorption models. Each equation can be expressed as follows:
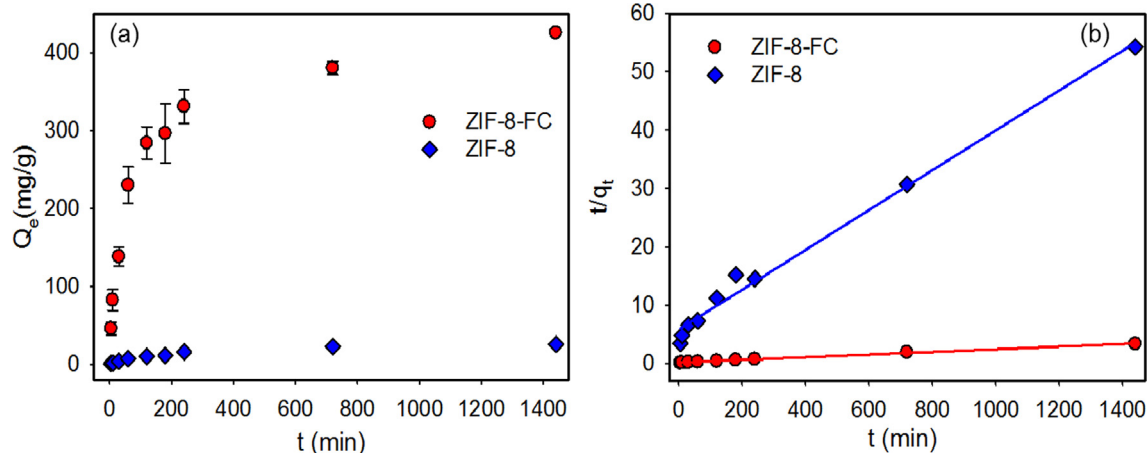

Fig. 4. (a) Adsorption kinetics of ZIF−8 and ZIF-8-FC, and (b) the results fitted by the pseudo-second-order kinetic model (C_o = 500 mg L^{-1}, V/m = 1000 mL g^{-1}, pH = 7, T = 298 K).

Table 1
Kinetic parameters for the Cs^+ adsorption on ZIF-8 and ZIF-8-FC.

Material	$q_{e,exp}$ (mg/g)	Pseudo-first-order			Pseudo-second-order		
		$q_{e,cal}$ (mg/g)	K_1 (min^{-1})	R^2	$q_{e,cal}$ (mg/g)	K_2 (g mg^{-1}min^{-1})	R^2
ZIF-8	26.53 ± 1.87	23.46	2.9×10^{-3}	0.986	26.54	2.1×10^{-4}	0.990
ZIF-8-FC	426.28 ± 2.57	266.51	2.8×10^{-3}	0.838	422.42	3.6×10^{-5}	0.998

Langmuir equation:

$$q_e = \frac{q_m K_L C_e}{1 + K_L C_e} \tag{5}$$

Freundlich equation:

$$q_e = K_F C_e^{\frac{1}{n_F}} \tag{6}$$

Sips equation:

$$q_e = \frac{q_m K_S C_e^{n_S}}{1 + K_S C_e^{n_S}} \tag{7}$$

where q_e (mg g^{-1}) is the amount Cs^+ adsorbed at an equilibrium concentration; C_e (mL g^{-1}) is the equilibrium concentration; q_m is the theoretical maximum adsorption capacity of Cs^+ in mg g^{-1}; K_L, K_S is the Langmuir and Sips equilibrium constant in L mg^{-1}, which is related to the free energy of the exchange; K_F (mg g^{-1}) and n_F are the empirical constants of the Freundlich model; and n_S is a constant related to heterogeneity system [40].

The relationships between the Cs^+ equilibrium concentration and the adsorption capacity are shown in Fig. 5a. The adsorption capacity of ZIF-8-FC was much higher than that of ZIF-8. The calculated isotherm parameters (Table 2) show that both ZIF-8 and ZIF-8-FC were well fitted by the Sips model, with R^2 values of 0.9666 and 0.9709, respectively.

ZIF-8-FC showed a much higher q_m of 422.42 mg g^{-1} than that of ZIF-8 (26.54 mg g^{-1}), which was among the highest of the various Cs^+ adsorbents. The adsorption capacity of ZIF-8-FC increased significantly because of the FC functionalization. In a previous report, KZFC exhibited good adsorption performance for Cs^+, which was controlled by diffusion, accessibility to reactive sites, and the surface parameters [2]. Here, the adsorption capacity of ZIF-8-FC was even higher than that of KZFC (360 mg g^{-1}), unlike the simple mixture of HKUST-1 and KNiFC [22,41]. This can be attributed to the higher surface area and more porous structure of ZIF-8-FC relative to the properties of KZFC [30]. From the XRD results, we also observed that the crystal size of FC in ZIF-8-FC was negligible. This prevented the hindrance of the Cs^+ migration within the crystal, indicating that additional FC sites were utilized for Cs^+ binding by rapid diffusion [42].

Fig. S6 shows the removal efficiency of Cs by ZIF-8 and ZIF-8-FC at various initial concentrations. ZIF-8-FC showed a removal efficiency of over 95% from the initial concentration of 10 to 300 mg L^{-1}. This result implies that ZIF-8-FC can be used to remove various amounts of Cs^+. The maximum adsorption capacities, q_m, and distribution coefficients, K_d, of various adsorbents in DI water for Cs^+ adsorption are summarized in Fig. 5b. ZIF-8-FC exhibited a
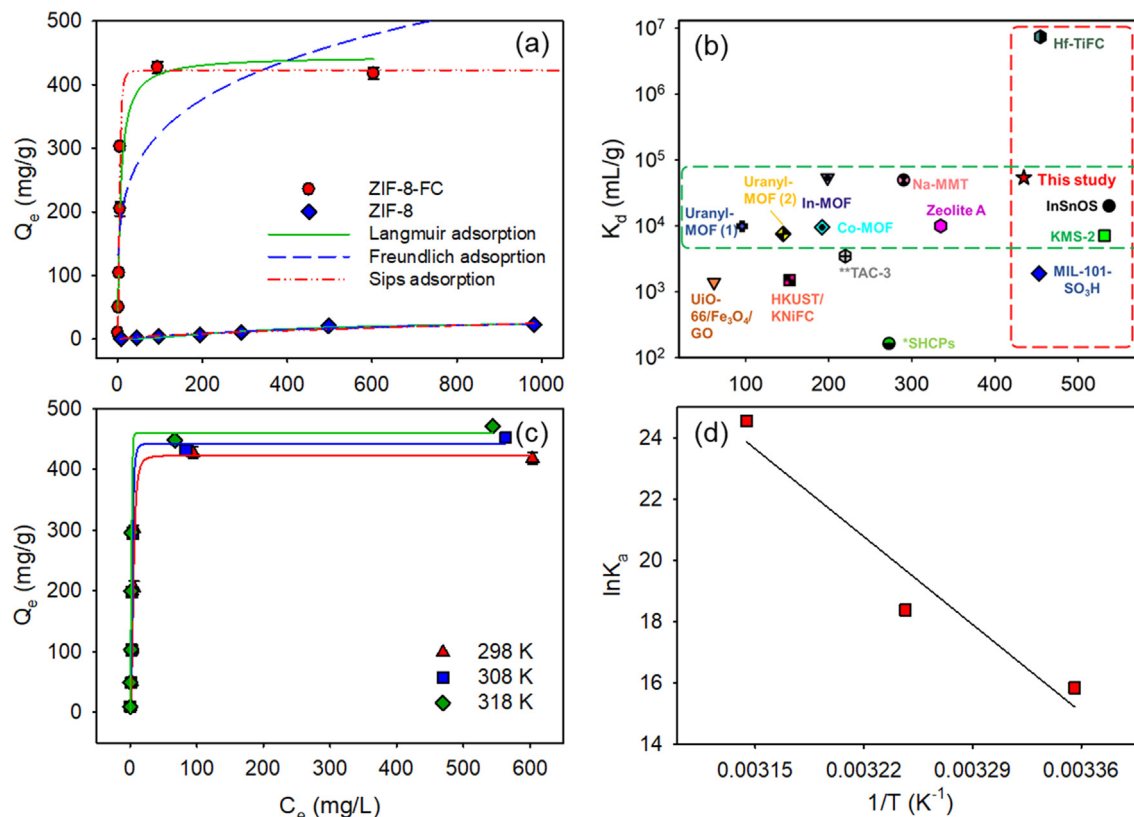

Fig. 5. (a) Adsorption isotherms of ZIF–8 and ZIF-8-FC, (b) Q_{max} (mg g^{-1}) and K_d (mL g^{-1}) values in DI water of various adsorbents (*K_d value from kinetic data; **Q_e (mg g^{-1})); (c) Thermodynamic adsorption isotherms of ZIF-8-FC (V/m = 1000 mL g^{-1}, contact time = 24 h, T = 298 K), (d) plot of ln K_a versus 1/T.

Table 2
Isotherm parameters for the adsorption of Cs⁺.

	Parameters	ZIF-8	ZIF-8-FC
Langmuir	q_m (mg g^{-1})	43.54	445.19
	K_s (L mg^{-1})	0.0013	0.1485
	R^2	0.9484	0.9024
Freundlich	K_F (mg g^{-1})	0.2640	119.589
	$1/n$	0.6586	0.2167
	R^2	0.9207	0.6918
Sips	q_m (mg g^{-1})	26.54	422.42
	K (L mg^{-1})	2.63×10^{-5}	0.0126
	n_S	1.8341	2.7214
	R^2	0.9666	0.9709

higher q_m value than most of the functionalized MOFs except MIL-101-SO₃H (453 mg g^{-1}) [21]. Specifically, the q_m was almost 3 times that of the composite obtained by simply mixing the MOF with MFC, which is HKUST-1/KNiFC [22]. This confirmed the originality and excellence of ZIF-8-FC. Metal chalcogenides, KMS-2 (531.74 mg g^{-1}) [15], hf-TiFC (454 mg g^{-1}) [43], and Indium Tin Oxysulfide (InSnOS) (537.7 mg g^{-1}) [44] showed relatively high q_m values. To evaluate the performance of the adsorbent, the selectivity of the adsorbent should be considered in addition to q_m. Furthermore, the q_m values of the various MFCs supported on various materials are listed in Table S3. Compared to other materials, ZIF-8-FC is a competitive adsorbent because of its high adsorption capacity for Cs⁺.

3.2.5. Adsorption thermodynamics

The effect of temperature on Cs⁺ adsorption was investigated between temperatures of 298 and 318 K. Fig. 5c shows that the Cs⁺ uptake increases with the temperature. This implies that a higher temperature is favorable for Cs⁺ adsorption. The fitting of the van't Hoff equation and thermodynamic parameters of the Cs⁺ adsorption on ZIF-8-FC are shown in Fig. 5d and Table 3, respectively. The thermodynamic parameters of the adsorption process are calculated by following equation:

The Gibb free energy ($\Delta G°$):

$$\Delta G° = -RT\ln K_a \tag{8}$$

where K_a is the equilibrium constant of Cs⁺ adsorption, T is the absolute temperature (K), and R is a gas constant (8.314 J mol^{-1} K^{-1}). The relationships between $\Delta G°$ and the enthalpy change ($\Delta H°$) and entropy change ($\Delta S°$) of adsorption are calculated as follows:

$$\Delta G° = \Delta H° - T\Delta S° \tag{9}$$

Substituting Eq. (8) into Eq. (9) gives:

$$\ln K_a = \frac{\Delta S°}{R} - \frac{\Delta H°}{RT} \tag{10}$$

The plot of ln K_a versus $1/T$ is a straight line which is used to calculate the values of $\Delta H°$ and $\Delta S°$ from the slope and intercept of Eq. (10).

Table 3 shows that the values of $\Delta G°$ were negative at all cases and decreased as temperature increased. This suggests that the adsorption was spontaneous and favorable at higher temperatures.

Positive values of $\Delta H°$ indicated an endothermic reaction. A positive $\Delta S°$ value implied an increasing randomness at the solid/liquid interface during the adsorption process [27].

3.2.6. Competition with other ions

The distribution coefficient, K_d, is the popular expression of the adsorption selectivity. The relatively large K_d value indicates a relatively high selectivity for Cs⁺. The maximum K_d value of ZIF-8-FC was 5.3×10^4 mL g^{-1} in DI water (Fig. 5b). In general, a material with a K_d value higher than 10^4 mL g^{-1} is considered to be an excellent adsorbent [44]. Fig. 6 shows the K_d value results and removal efficiency (R, %) at various concentrations of Na⁺, K⁺, Mg²⁺ and Ca²⁺. ZIF-8-FC maintained a removal efficiency of 98% or greater and the K_d values were higher than 5.4×10^4 mL g^{-1} at concentrations of up to 0.01 M, regardless of the cation type. At a concentration of 0.1 M, the K_d values were greater 3.9×10^4 mL g^{-1}, whereas the removal efficiencies were higher than 97%. At a competing ion concentration of 1.0 M, the K_d decreased to 1.0×10^4 mL g^{-1}, especially for K⁺. As shown in Fig. S7, the K_d and R% values were affected in the following order: K⁺ > Na⁺ > Ca²⁺ > Mg²⁺. This result can be attributed to the similar hydrated radius of K⁺ (3.30 Å) and Cs⁺ (3.25 Å) relative to those of the other cations [10].

In real applications, many species other than the target pollutant are present in the wastewater. These species can deteriorate the performance of the adsorbent, which is dissimilar to what occurs in DI water. We used ASW because it has a high ionic strength with various cations, such as Na⁺, K⁺, Ca²⁺, and Mg²⁺, and anions, such as HCO₃⁻, CO₃²⁻, SO₄²⁻, HPO₄²⁻, and Cl⁻, which have a strong effect on the selective capture of Cs⁺ [44,45]. In addition, seawater is also contaminated by Cs⁺. The values of K_d are assessed at various concentrations of Cs⁺ in water and ASW. ZIF-8-FC exhibited a very high K_d value of 4.3×10^4 mL g^{-1} for Cs⁺ in the ASW. This value is only 20% lower than the value in DI water, which is remarkable. The K_d values of the various adsorbents at various conditions are listed in Table S4. MIL-101-SO₃H, which exhibited a high q_m, showed a very low K_d value even at relatively low salt concentrations. KMS-2 and InSnOS showed similar low K_d values. The K_d value of 4.3×10^4 mL g^{-1} for Cs⁺ was the best among the MOFs in the ASW. In the MOF–MFC composites, the K_d value of ZIF-8-FC was ~100 times higher than that of HKUST-1/KNiFC, even at a higher Na⁺ concentration. The reasons for these results are discussed in the mechanism section.

Under real conditions, the concentration of Cs⁺ can be very low; therefore, we performed an adsorption test at low concentrations of Cs⁺ in ASW. The K_d values at 5 ppb, 10 ppb, and 10 ppm of Cs⁺ were 1.2×10^3, 4.8×10^3, and 6.8×10^3 mL/g, respectively (Fig. S8). The K_d value of ZIF-8-FC, at 10 ppb of Cs⁺, under extremely high concentrations of competing ions, was still higher than those of most materials listed in Table S4. For example, K_d of ZIF-8-FC was higher than that of Uranyl MOFs (4.1×10^3 and 6.32×10^2 mL/g), TAC (1.5×10^3 mL/g), and Na-treated MMT (1.5×10^3 mL/g).

3.2.7. Adsorption mechanism

The adsorption mechanism of Cs⁺ on ZIF-8 may be the surface complexation between the Zn–O bond and the coordination bonds, which occurs between the un-bonded nitrogen atoms and Cs⁺ [46].
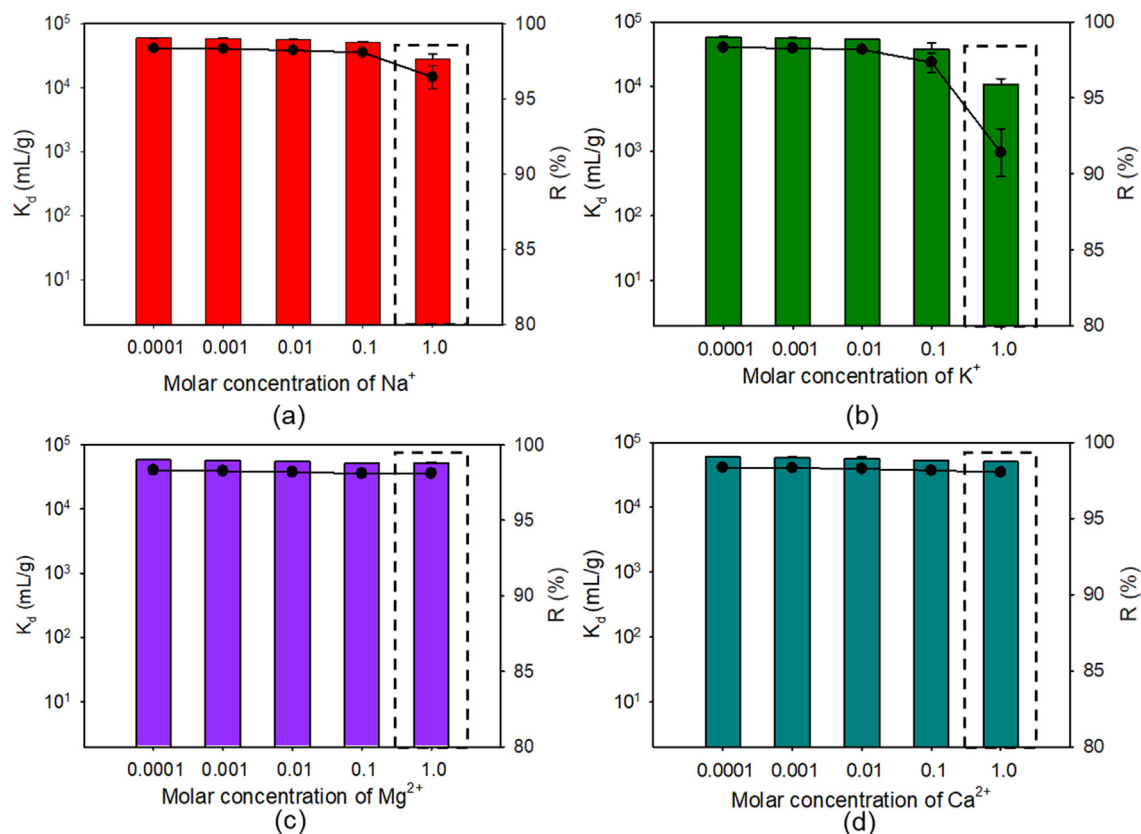
Table 3
Isotherm adsorption and the thermodynamic adsorption parameters of Cs⁺ at different temperatures.

T (K)	K_L (L mg^{-1})	q_m (mg g^{-1})	R^2	$\triangle G°$ (kJ mol^{-1})	$\triangle H°$ (kJ mol^{-1})	$\triangle S°$ (kJ mol^{-1}K^{-1})
298	0.086	422.42	0.9978	−39.18	340.88	1.27
308	0.130	454.55	0.9996	−40.50		
318	0.168	476.19	0.9993	−41.81		

Fig. 6. The distribution coefficient and removal efficiency of ZIF-8-FC for various competing ions: (a) Na$^+$; (b) K$^+$; (c) Mg^{2+} and (d) Ca^{2+}; (C$_o$ = 300 mg L^{-1}, V/m = 1000 mL g^{-1}, pH = 7, T = 298 K).

Moreover, electrostatic attraction at a high pH further improved the Cs$^+$ adsorption [47]. However, these mechanisms are not significant because the adsorption capacity of ZIF-8 is low.

The high maximum adsorption capacity and selectivity of ZIF-8-FC can be explained in four ways. First, ion exchange between Cs$^+$ and K$^+$ is the most general mechanism for various adsorbents [2,42]. To confirm this, ICP analysis was used to determine the K$^+$ and Cs$^+$ contents before and after adsorption. As shown in Table S5, the concentrations of K$^+$ and Cs$^+$ in the solution were measured before and after the adsorption by ZIF-8-FC(0.8) at two initial Cs concentrations. After the 24 h adsorption process, the concentration of K$^+$ increased whereas that of Cs$^+$ decreased. At an initial Cs$^+$ concentration of 205 ppm, the molar ratio of the released K$^+$ to the adsorbed Cs$^+$ was 2.464. The adsorption of H$^+$ on ZIF-8-FC may explain this ratio because an increase in pH was observed. At an initial Cs$^+$ concentration of 505 ppm, this molar ratio was 1.161. As the initial Cs$^+$ concentration increased, the ratio of K$^+$ to Cs$^+$ moved closer to 1. These results indicate that ZIF-8-FC prefers to adsorb to Cs$^+$ over H$^+$, which supports the high adsorption capacity that occurs over a wide range of pH values, as shown in Fig. 3b. Therefore, we confirmed that the main adsorption mechanism is ion exchange. However, further study is necessary because the Cs$^+$ adsorption mechanism of MFCs remains unclear and strongly depends on the compositions and structure of the MFC [43].

Ion exchange usually affects the maximum adsorption capacity rather than the selectivity. When there is no other mechanism present, the selectivity of the adsorbent may be low regardless of the maximum adsorption capacity. Hence, other mechanisms are required. Second, the window size of MFC (3.2 Å) is well fitted with the size of hydrated Cs$^+$ (3.29 Å) [2]. Incidentally, the sizes of hydrated Mg^{2+}, Ca^{2+}, Na$^+$, and K$^+$ are 4.28, 4.12, 3.58, and 3.31 Å, respectively [32]. Therefore, the exclusion of these cations based

on the window size of MFC can result in a relatively high selectivity of ZIF-8-FC.

Third, the soft cyanide anion prefers soft Cs$^+$ to hard Na$^+$, K$^+$, Mg^{2+}, and Ca^{2+} [48]. In aqueous solutions, the chemical affinity can be explained by the chemical hardness of the metal ion and adsorbent. When the hardness between the adsorbate ion and the adsorbent is compatible, they form a strong bond and preserve the complex [49]. The chemical hardness decreases in the following order: Mg^{2+} > Na$^+$ > Ca^{2+} > K$^+$ > Cs$^+$, with values of 32.55, 21.08, 19.52, 13.64, and 10.6 eV, respectively [50].

These three factors also apply to other MFCs that showed lower q_m values. Therefore, there is a final explanation for the properties of ZIF-8-FC: enhanced Cs$^+$ transport due to the higher specific surface area, small FC crystal size, and partial hollow structure of ZIF-8-FC. The MFC crystal without vacancies limited the Cs$^+$ adsorption due to limited Cs$^+$ migration in the crystal [42]. Therefore, the small crystal size of the KZFC distributed in ZIF-8-FC with a relatively high surface area and a partial hollow structure resulted in the enhanced diffusion of Cs$^+$.

4. Conclusions

We synthesized a novel ZIF-8-FC composite made of ZIF-8 functionalized with FC via a simple synthesis procedure at room temperature. ZIF-8 showed a maximum adsorption capacity of 26.54 mg g^{-1} for Cs$^+$. After functionalization with FC, ZIF-8-FC showed a maximum adsorption capacity of 422.42 mg g^{-1} for Cs$^+$. ZIF-8-FC also exhibited a high K_d of 5.3 × 10^4 mL g^{-1} in DI water. Even in ASW with high concentrations of Na$^+$, K$^+$, Ca^{2+} and Mg^{2+}, ZIF-8-FC showed excellent Cs$^+$ selectivity with a K_d value of 4.3 × 10^4 mL g^{-1}. The isotherm and kinetic adsorption showed that ZIF-8-FC followed the Sips model and pseudo-second-order kinetic

model, which implied multilayer chemical adsorptions. Furthermore, the adsorption process is favorable at increased temperatures. The adsorption performance was quite stable across a wide range of pH values. In addition to the advantages of MFC, ZIF-8-FC had high surface area and small KZFC crystal size, resulting in the enhanced diffusion of Cs^+ and, consequently, a high adsorption capacity. Considering the factors above, ZIF-8-FC can be applied to remove Cs^+ in various environments.

Funding Sources

CRediT authorship contribution statement

Quynh Thi Ngoc Le: Conceptualization, Methodology, Writing - original draft. **Kuk Cho:** Conceptualization, Supervision, Writing - review & editing.

Declaration of Competing Interest

The authors declare that they have no known competing financial interests or personal relationships that could have appeared to influence the work reported in this paper.

Acknowledgment

Appendix A. Supplementary material

Supplementary data to this article can be found online at https://doi.org/10.1016/j.jcis.2020.08.017.

References

[1] A.M. James, S. Harding, T. Robshaw, N. Bramall, M.D. Ogden, R. Dawson, Selective environmental remediation of strontium and cesium using sulfonated hyper-cross-linked polymers (SHCPs), ACS Appl. Mater. Interfaces 11 (25) (2019) 22464–22473.

[2] T. Vincent, C. Vincent, E. Guibal, Immobilization of metal hexacyanoferrate ion-exchangers for the synthesis of metal ion sorbents—a mini-review, Molecules 20(11) (2015) 20582–20613.

[3] J. Ai, F.-Y. Chen, C.-Y. Gao, H.-R. Tian, Q.-J. Pan, Z.-M. Sun, Porous Anionic Uranyl–organic networks for highly efficient Cs^+ adsorption and investigation of the mechanism, Inorg. Chem. 57 (8) (2018) 4419–4426.

[4] A. Courti, P. Bouisset, P. Chevallier, Beta spectrometry for environmental radioactivity measurements, Ecorad (2001).

[5] A. Oancea, A. Popescu, M. Radulescu, V. Weber, E. Pincovschi, M. Cox, Kinetics of cesium and strontium ions removal from wastewater on gel and macroporous resins, Solvent Extr. Ion Exch. 26 (3) (2008) 217–239.

[6] H.-R. Yu, J.-Q. Hu, Z. Liu, X.-J. Ju, R. Xie, W. Wang, L.-Y. Chu, Ion-recognizable hydrogels for efficient removal of cesium ions from aqueous environment, J. Hazard. Mater. 323 (2017) 632–640.

[7] H. Rogers, J. Bowers, D. Gates-Anderson, An isotope dilution–precipitation process for removing radioactive cesium from wastewater, J. Hazard. Mater. 243 (2012) 124–129.

[8] S. Rao, B. Paul, K. Lal, S. Narasimhan, J. Ahmed, Effective removal of cesium and strontium from radioactive wastes using chemical treatment followed by ultra filtration, J. Radioanal. Nucl. Chem. 246 (2) (2000) 413–418.

[9] W.R. Wilmarth, G.J. Lumetta, M.E. Johnson, M.R. Poirier, M.C. Thompson, P.C. Suggs, N.P. Machara, Waste-pretreatment technologies for remediation of legacy defense nuclear wastes, Solvent Extr. Ion Exch. 29 (1) (2011) 1–48.

[10] H.A. Alamudy, K. Cho, Selective adsorption of cesium from an aqueous solution by a montmorillonite-prussian blue hybrid, Chem. Eng. J. 349 (2018) 595–602.

[11] J. Cheng, J. Liang, L. Dong, J. Chai, N. Zhao, S. Ullah, H. Wang, D. Zhang, S. Imtiaz, G. Shan, G. Zheng, Self-assembly of 2D-metal–organic framework/graphene oxide membranes as highly efficient adsorbents for the removal of Cs^+ from aqueous solutions, RSC Adv. 8 (71) (2018) 40813–40822.

[12] X.-H. Qi, K.-Z. Du, M.-L. Feng, J.-R. Li, C.-F. Du, B. Zhang, X.-Y. Huang, A two-dimensionally microporous thiostannate with superior Cs^+ and Sr^{2+} ion-exchange property, J. Mater. Chem. A 3 (10) (2015) 5665–5673.

[13] H.Y. Lee, H.S. Kim, H.-K. Jeong, M. Park, D.-Y. Chung, K.-Y. Lee, E.-H. Lee, W.T. Lim, Selective removal of radioactive cesium from nuclear waste by zeolites: on the origin of cesium selectivity revealed by systematic crystallographic studies, J. Phys. Chem. C 121 (19) (2017) 10594–10608.

[14] M.J. Manos, M.G. Kanatzidis, Highly efficient and rapid Cs^+ uptake by the layered metal sulfide $K_{2x} Mn_x Sn_{3−x}S_6$ (KMS-1), J. Am. Chem. Soc. 131 (18) (2009) 6599–6607.

[15] J.L. Mertz, Z.H. Fard, C.D. Malliakas, M.J. Manos, M.G. Kanatzidis, Selective Removal of Cs^+, Sr^{2+}, and Ni^{2+} by $K_{2x}Mg_xSn_{3−x}S_6$ (x= 0.5–1)(KMS-2) relevant to nuclear waste remediation, Chem. Mater. 25(10) (2013) 2116–2127.

[16] Y.K. Kang, H. Lee, T.D.C. Ha, J.K. Won, H. Jo, K.M. Ok, S. Ahn, B. Kang, K. Ahn, Y. Oh, M.-G. Kim, Thiostannate coordination transformation-induced self-crosslinking chalcogenide aerogel with local coordination control and effective Cs^+ remediation functionality, J. Mater. Chem. A 8 (6) (2020) 3468–3480.

[17] S. Solbrå, N. Allison, S. Waite, S.V. Mikhalovsky, A.I. Bortun, L.N. Bortun, A. Clearfield, Cesium and strontium ion exchange on the framework titanium silicate $M_2Ti_2O_3SiO_4.nH_2O$ (M= H, Na), Environ. Sci. Technol. 35(3) (2001) 626–629.

[18] Y. Liu, P. Na, J. Chen, Y. Xie, Magnetic $K_2Zn_3[Fe(CN)_6]_2$ @ Ni-P composites for highly selective cesium separation, Colloids Surf., A 550 (2018) 99–107.

[19] A. Pournara, A. Margariti, G.D. Tarlas, A. Kourtelaris, V. Petkov, C. Kokkinos, A. Economou, G.S. Papaefstathiou, M.J. Manos, A Ca $^{2+}$ MOF combining highly efficient sorption and capability for voltammetric determination of heavy metal ions in aqueous media, J. Mater. Chem. A 7 (25) (2019) 15432–15443.

[20] P. Kumar, A. Pournara, K.-H. Kim, V. Bansal, S. Rapti, M.J. Manos, Metal-organic frameworks: challenges and opportunities for ion-exchange/sorption applications, Prog. Mater Sci. 86 (2017) 25–74.

[21] B. Aguila, D. Banerjee, Z. Nie, Y. Shin, S. Ma, P.K. Thallapally, Selective removal of cesium and strontium using porous frameworks from high level nuclear waste, Chem. Commun. 52 (35) (2016) 5940–5942.

[22] S. Naeimi, H. Faghihian, Performance of novel adsorbent prepared by magnetic metal-organic framework (MOF) modified by potassium nickel hexacyanoferrate for removal of Cs^+ from aqueous solution, Sep. Purif. Technol. 175 (2017) 255–265.

[23] Y.-J. Gao, M.-L. Feng, B.o. Zhang, Z.-F. Wu, Y. Song, X.-Y. Huang, An easily synthesized microporous framework material for the selective capture of radioactive Cs^+ and Sr^{2+} ions, J. Mater. Chem. A 6 (9) (2018) 3967–3976.

[24] Y. Wang, Z. Liu, Y. Li, Z. Bai, W. Liu, Y. Wang, X. Xu, C. Xiao, D. Sheng, J. Diwu, J. Su, Z. Chai, T.E. Albrecht-Schmitt, S. Wang, Umbellate distortions of the uranyl coordination environment result in a stable and porous polycatenated framework that can effectively remove cesium from aqueous solutions, J. Am. Chem. Soc. 137 (19) (2015) 6144–6147.

[25] N.A.H.M. Nordin, S.M. Racha, T. Matsuura, N. Misdan, N.A.A. Sani, A.F. Ismail, A. Mustafa, Facile modification of ZIF-8 mixed matrix membrane for CO_2/CH_4 separation: synthesis and preparation, RSC Adv. 5 (54) (2015) 43110–43120.

[26] M. Jian, B. Liu, R. Liu, J. Qu, H. Wang, X. Zhang, Water-based synthesis of zeolitic imidazolate framework-8 with high morphology level at room temperature, RSC Adv. 5 (60) (2015) 48433–48441.

[27] C. Wang, T. Zheng, R. Luo, C. Liu, M. Zhang, J. Li, X. Sun, J. Shen, W. Han, L. Wang, In situ growth of ZIF-8 on PAN fibrous filters for highly efficient U(VI) removal, ACS Appl. Mater. Interfaces 10 (28) (2018) 24164–24171.

[28] M. Niknam Shahrak, M. Ghahramaninezhad, M. Eydifarash, Zeolitic imidazolate framework-8 for efficient adsorption and removal of Cr(VI) ions from aqueous solution, Environ. Sci. Pollut. Res. 24 (10) (2017) 9624–9634.

[29] Y. Huang, X. Zeng, L. Guo, J. Lan, L. Zhang, D. Cao, Heavy metal ion removal of wastewater by zeolite-imidazolate frameworks, Sep. Purif. Technol. 194 (2018) 462–469.

[30] V. Jassal, U. Shanker, B.S. Kaith, S. Shankar, Green synthesis of potassium zinc hexacyanoferrate nanocubes and their potential application in photocatalytic degradation of organic dyes, RSC Adv. 5 (33) (2015) 26141–26149.

[31] Y.-N. Wu, M. Zhou, B. Zhang, B. Wu, J. Li, J. Qiao, X. Guan, F. Li, Amino acid assisted templating synthesis of hierarchical zeolitic imidazolate framework-8 for efficient arsenate removal, Nanoscale 6 (2) (2014) 1105–1112.

[32] E.R. Nightingale Jr., Phenomenological Theory of Ion Solvation. Effective Radii of Hydrated Ions, J. Phys. Chem. 63 (9) (1959) 1381–1387.

[33] B. Saparov, D.B. Mitzi, Organic–inorganic perovskites: structural versatility for functional materials design, Chem. Rev. 116 (7) (2016) 4558–4596.

[34] A. Omura, Y. Moritomo, Cs^+ Trapping in size-controlled nanospaces of hexacyanoferrates, Appl. Phys. Express 5 (5) (2012) 057101.

[35] D. Gao, Y. Dong, W. Li, Y. Li, Adsorption of cesium(I) using potassium zinc hexacyanoferrate and its application in simulated oilfield water, Curr. Chem. Res. 1 (1) (2011) 44–49.

[36] A. Chakraborty, S. Laha, K. Kamali, C. Narayana, M. Eswaramoorthy, T.K. Maji, In situ growth of self-assembled ZIF-8–aminoclay nanocomposites with enhanced surface area and CO_2 uptake, Inorg. Chem. 56 (16) (2017) 9426–9435.

[37] J. Li, Y.-N. Wu, Z. Li, B. Zhang, M. Zhu, X. Hu, Y. Zhang, F. Li, Zeolitic imidazolate framework-8 with high efficiency in trace arsenate adsorption and removal from water, J. Phys. Chem. C 118 (47) (2014) 27382–27387.

[38] K. Gupta, B. Yuan, C. Chen, N. Varnakavi, M.-L. Fu, $K_{2x}Mn_xSn_{3-x}S_6$ (x = 0.5–0.95) (KMS-1) immobilized on the reduced graphene oxide as KMS-1/r-GO aerogel to effectively remove Cs^+ and Sr^{2+} from aqueous solution, Chem. Eng. J. 369 (2019) 803–812.

[39] J.-P. Simonin, On the comparison of pseudo-first order and pseudo-second order rate laws in the modeling of adsorption kinetics, Chem. Eng. J. 300 (2016) 254–263.

[40] D.D. Do, Adsorption Analysis: Equilibria and Kinetics, Imperial College Press. London, 1998.

[41] C. Loos-Neskovic, M. Fedoroff, Exchange mechanism of alkaliions on zinc ferrocyanides, Reactive Polymers, Ion Exchangers, Sorbents 7 (2–3) (1988) 173–183.

[42] A. Takahashi, H. Tanaka, K. Minami, K. Noda, M. Ishizaki, M. Kurihara, H. Ogawa, T. Kawamoto, Unveiling Cs-adsorption mechanism of Prussian blue analogs: Cs^+-percolation via vacancies to complete dehydrated state, RSC Adv. 8 (61) (2018) 34808–34816.

[43] H.-M. Yang, C.W. Park, I. Kim, I.-H. Yoon, Hollow flower-like titanium ferrocyanide structure for the highly efficient removal of radioactive cesium from water, Chem. Eng. J. 392 (2020) 123713.

[44] L. Wang, H. Pei, D. Sarma, X.-M. Zhang, K. MacRenaris, C.D. Malliakas, M.G. Kanatzidis, Highly selective radioactive $^{137}Cs^+$ capture in an open-framework

[45] T. Carey, C.D. Williams, D.J. McArthur, T. Malkinson, O.R. Thompson, A. Baidak, L. Murtagh, G. Glodan, S.P. Morgan, A.W. Banford, Removal of Cs, Sr, U and Pu species from simulated nuclear waste effluent using graphene oxide, J. Radioanal. Nucl. Chem. 317 (1) (2018) 93–102.

[46] Y. Wu, B. Li, X. Wang, S. Yu, H. Pang, Y. Liu, X. Liu, X. Wang, Magnetic metal-organic frameworks (Fe_3O_4@ZIF-8) composites for U(VI) and Eu(III) elimination: simultaneously achieve favorable stability and functionality, Chem. Eng. J. 378 (2019) 122105.

[47] Y. Zhang, Z. Xie, Z. Wang, X. Feng, Y. Wang, A. Wu, Unveiling the adsorption mechanism of zeolitic imidazolate framework-8 with high efficiency for removal of copper ions from aqueous solutions, Dalton Trans. 45 (32) (2016) 12653–12660.

[48] R.G. Pearson, Of the American chemical society, J. Am. Chem. Soc. 85 (22) (1963) 3533–3539.

[49] Y.J. Suh, J.W. Chae, H.D. Jang, K. Cho, Role of chemical hardness in the adsorption of hexavalent chromium species onto metal oxide nanoparticles, Chem. Eng. J. 273 (2015) 401–405.

[50] R.G. Pearson, Absolute electronegativity and hardness: application to inorganic chemistry, Inorg. Chem. 27 (4) (1988) 734–740.

oxysulfide based on supertetrahedral cluster, Chem. Mater. 31 (5) (2019) 1628–1634.